Structure and Properties for Biomass-Based Polyester Blends of PLA and PBS

Tadashi Yokohara and Masayuki Yamaguchi*

School of Materials Science,
Japan Advanced Institute of Science and Technology
1-1 Asahidai, Nomi, Ishikawa 923-1292 JAPAN

*Corresponding to
Masayuki Yamaguchi
School of Materials Science, Japan Advanced Institute of Science and Technology
1-1 Asahidai, Nomi, Ishikawa 923-1292 Japan
Phone +81-761-51-1621, Fax +81-761-51-1625
E-mail m_yama@jaist.ac.jp

Abstract

Structure and properties are studied for binary blends composed of poly(lactic acid) (PLA) and poly(butylene succinate) (PBS). The rheological measurements in the molten state reveal that the entanglement molecular weight of PLA is lower than that of PBS. Further, the interfacial tension of the immiscible blend system is evaluated employing a rheological emulsion model and found to be 3.5 [mN/m]. Moreover, thermal analysis directly detects that addition of PBS enhances the crystallization of PLA even though PBS is in a molten state. Further, the cold crystallization for quenched blends occurs at lower temperature than that for a quenched PLA. This would be attributed to the nucleating ability of PBS, leading to generation of PLA crystallites during the quench operation.

Key words: polylactide; polymer blend; crystallization; rheological properties; interfacial tention

INTRODUCTION

Great attention has been focused on biomass-based polyesters derived from renewable resources, such as poly(lactic acid) PLA, poly(butylene succinate) PBS, and poly(3-hydroxybutyrate) PHB, because of a rapid growth of intensive interest in the global environment [1-3]. In particular, the annual supply of PLA is expected to increase rapidly in near future owing to the various attractive properties, such as high rigidity, biodegradability, and biocompatibility. For an immense consumption of PLA, however, considerable efforts will be required to overcome the following defects; (1) slow crystallization, (2) poor heat resistance, and (3) mechanical brittleness.

One of the most famous techniques to enhance the crystallization rate is blending ultrafine layered silicate, so-called nanoclay [4,5]. The composite of PLA with the nanoclay exhibits excellent heat resistance due to high degree of crystallinity. Further, various types of nucleating agents, including organic and inorganic, have been developed for a similar purpose, which is significantly important from the viewpoints of processing, *e.g.*, cycle time at injection-molding and out-put rate at extrusion [6-9]. Furthermore, extensive investigations on polymer blend technology have been also carried out. Yamane et al. firstly found from the precise rheological measurements that small addition of an enantiomer, *i.e.*, poly(D-lactic acid) PDLA, greatly enhances the crystallization rate of poly(L-lactic acid) PLLA [10], because the stereocomplex crystallites having a higher melting point act as nucleating agents for the rest of a molten PLLA [11]. They also revealed that strain-hardening behavior in elongational viscosity, one of the most important rheological properties for polymer processing, is

prominent for the blend. Further, Anderson and Hillmyer carried out melt blending of PLLA and PDLA and confirmed that the blend shows high crystallization rate [12]. Moreover, a number of studies on PLA/PHB blends have been reported [13-16]. According to them, PLA is immiscible with PHB, when both components have high molecular weights. Further, it was found that mechanical properties of the blends are intermediate between those of the individual pure components. PBS is also studied as a modifier for PLA, because both materials exhibit biodegradablity. Although Park and Im reported that PLA is miscible with PBS in the amorphous region from the results of thermal analysis [17], recent studies have concluded that PLA is immiscible with PBS [18-21]. Chen et al. found that a reactive organoclay with glycidyl functionality acts as a compatibilizer for PLA/PBS blends and enhances the tensile properties such as tensile modulus and elongation at break [20]. Furthermore, Takagi et al. [18] and Shibata et al. [21] clarified that adding PBS enhances the cold crystallization of PLA, *i.e.,* increase in the crystallization rate of PLA during heating process for a quenched sample [22]. This phenomenon should be notified because PBS would act as nuclei for PLA crystallization, although the nucleating effect of PBS during the cooling process has not been directly detected yet to the best of our knowledge. The result suggests that characteristics of phase-separated structure, such as the size and number of dispersed PBS particles in PLA matrix, have a significant influence on the crystallization rate of PLA and therefore the mechanical properties. In general, domain size of an immiscible polymer blend is determined by interfacial tension, viscosity ratio, and applied external force [23-27]. In other words, the morphology is predictable from the material parameters as well as the mixing condition. The interfacial tension between PLA and PBS is, however, unknown, which restricts the material design for the biomass-based

blends.

In this study, the interfacial tension is evaluated by means of rheological measurements with the characterization of basic viscoelastic parameters for PLA and PBS in the molten state. The obtained results will be important information on the material design for PLA/PBS blend system as well as the prediction of the adhesive properties between them. Further, the effect of blending PBS on the PLA crystallization is also investigated.

EXPERIMENTAL

Materials

The polymers used in this study were commercially available poly(lactic acid) (PLA), (Mitsui Chemicals, LACEA) and poly(butylene succinate) (PBS), (Mitsubishi Chemical, Gspla). Molecular weights and the distribution were evaluated by a gel permeation chromatography (Tosoh, HLC-8020) with TSK-GEL GMHXL as a polystyrene standard. Chloroform was employed as eluant at a flow rate of 1.0 ml/min and the sample concentration was 1.0 mg/ml. The number, weight, and z-average molecular weights are as follows; Mn = 1.5 x 10^5, Mw = 2.5 x 10^5, and Mz = 4.2 x 10^5 for PLA; and Mn = 5.0 x 10^4, Mw = 1.5 x 10^5, and Mz = 3.7 x 10^5 for PBS. The optical purity of L-lactic acid is about 96 %.

Sample Preparation

PLA and PBS were mixed together in a molten state at various blend ratios, *i.e.*, PLA/PBS=100/0, 95/5, 90/10, and 80/20 in weight fraction, with thermal stabilizers

such as a hindered phenol (Ciba, Irganox 1010) and a phosphate (Ciba, Irgafos 168). The amount of each thermal stabilizer used in the preparation was 0.5%. Compounding was performed by an internal batch mixer (Toyoseiki, Labo-plastmil) at 180 ºC for 3 min. The blade rotation speed was 40 rpm. Prior to melt-mixing, the polymers were dried under vacuum at 80 ºC for 4 h.

The obtained samples were compressed into flat sheets with 0.4 mm thickness by a laboratory compression-molding machine at 180 ºC under 10 MPa for 3 min. Then the sample was subsequently cooled at 40ºC in another compression-molding machine.

Measurements

The frequency dependence of oscillatory shear moduli in the molten state, such as shear storage modulus G' and loss modulus G'', were evaluated by a cone-and-plate rheometer (UBM, MR-500) under a nitrogen atmosphere to avoid thermal-oxidative degradation at various temperatures, *i.e.*, 160, 180, 200, and 220 ºC. The diameter of the cone is 25 mm and the cone-angle is 5 degree.

The temperature dependence of oscillatory tensile moduli in the solid state, such as tensile storage modulus E' and loss modulus E'', were measured employing a rectangular sample with 3 mm x 20 mm x 0.4 mm by a dynamic mechanical analyzer (UBM, E4000) in the temperature range between -80 and 170 ºC. The heating rate was 2 ºC/min and the applied frequency was 10 Hz.

The morphology of the blends was examined by a scanning electron microscope (SEM) (Hitachi, S4100). Prior to the observation, the surface of cryogenically fractured samples was coated by Pt-Pd.

Thermal analysis was conducted by a differential scanning calorimeter (DSC)

(Mettler, DSC820) under a nitrogen atmosphere. The samples were heated from room temperature to 180 ºC at a heating rate of 2 ºC/min. After holding at 180 ºC for 3 min, the samples were cooled down at a cooling rate of 2 ºC /min. The amount of the sample in an aluminum pan was approximately 10 mg weight.

The crystallization behavior of PLA and blends was observed also by an optical polarized microscope (Leica, DMLB HC) equipped with an automated hot-stage (Mettler, FP82HT). The sample films were sandwiched between cover glasses and heated up to 180 ºC. After holding at 180 ºC for 3 min, the sample was cooled down at a cooling rate of 2 ºC/min.

RESULTS AND DISCUSSION

Rheological Properties in Molten State

The master curves of frequency dependence of oscillatory shear moduli for PLA and PBS are shown in Figure 1. The reference temperature is 180 ºC.

[Figure 1]

The apparent flow activation energies, calculated from the horizontal shift factor using Arrhenius equation [28], are 67 [kJ/mol] for PLA and 43 [kJ/mol] for PBS.

As seen in the figure, G'' of PLA is higher than that of PBS employed. Further, the slope of G'' is 1.0 and that of G' is 2.0 in the low frequency region for both polymers. Therefore, the rheological parameters in the terminal zone, such as zero-shear viscosity η_0 and steady-state compliance J_e^0, are provided by the

following relations [28];

$$\eta_0 = \lim_{\omega \to 0} \frac{G''(\omega)}{\omega} \quad (1)$$

$$J_e^0 = \lim_{\omega \to 0} \frac{G'(\omega)}{G''(\omega)^2} \quad (2)$$

The zero-shear viscosity and steady-state compliance of PLA and PBS are calculated as follows; η_0 =3.1 x 10^3 [Pa s] and J_e^0 =3.0 x 10^{-5} [Pa^{-1}] for PLA; and η_0 =4.0 x 10^2 [Pa s] and J_e^0 =1.4 x 10^{-4} [Pa^{-1}] for PBS. Following the empirical relation (equation 3) proposed by Mills [28,29], the values of J_e^0 for the mono-disperse PLA and PBS are calculated to be 3.0 x 10^{-5} [Pa^{-1}] and 1.4 x 10^{-4} [Pa^{-1}], respectively.

$$J_e^0 \propto \left(\frac{Mz}{Mw} \right)^{3.7} \quad (3)$$

The result suggests that rubbery plateau modulus G_N^0 of PLA is higher than that of PBS, considering the following equation [28,30,31].

$$J_N^0 = \frac{1}{G_N^0} \propto J_e^0 \text{(monodisperse)} \quad (4)$$

where J_N^0 is the shear compliance associated with entanglement network. Based on the

analogy with the classical rubber elasticity theory [28,31], G_N^0 is proportional to the inverse of *Me*, *i.e.*, the average molecular weight between entanglement couplings.

$$G_N^0 = \frac{\rho RT}{Me} \tag{5}$$

where ρ is the density. Since the monodisperse PLA shows lower J_N^0 as discussed before, *Me* of PLA is lower than that of PBS.

Figure 2 shows the master curves of oscillatory shear moduli for PLA/PBS blends in the molten state at 180 ºC. The principle of time-temperature superposition is applicable to all blends, indicating that the molecular aggregation state and/or morphology in the blends are stable over the entire experimental regions of frequency and temperature. Further, there is a shoulder peak in the G' curve in the low frequency region for the blends with 10 and 20 wt% of PBS, suggesting the existence of long relaxation time. The long-time relaxation mechanism is ascribed to the recovery process from the deformed state by hydrodynamic force. As studied extensively by Oldroyd [32], Palierne [33,34], and Doi and Ohta [35], the interfacial tension between the continuous and dispersed phases is responsible for the recovery process, because the entanglement couplings between continuous and dispersed phases is so weak owing to considerably thin thickness of the interface region.

[Figure 2]

Palierne developed a constitutive equation of linear viscoelastic functions [33],

so-called “emulsion model”, for binary blends of immiscible viscoelastic fluids based on the pioneering work by Oldroyd [32], in which the effect of interfacial tension on the elastic response is considered as a dominant factor for the recovery process from deformed state of droplets. According to the emulsion model [33], oscillatory shear moduli in the molten state for immiscible polymer blends are described by those of the individual pure components, interfacial tension, and dispersed particle size. Therefore, the interfacial tension between two immiscible polymer melts can be evaluated by the linear viscoelastic properties and the dispersed particle size [33,34,36,37]. The emulsion model is given by the following relation:

$$G^*(\omega) = G_m^*(\omega)\frac{1+3\phi H(\omega)}{1-2\phi H(\omega)} \tag{6}$$

$$H(\omega) = \frac{4\left(\frac{\Gamma}{R_v}\right)\{2G_m^*(\omega)+5G_d^*(\omega)\}+\{G_d^*(\omega)-G_m^*(\omega)\}\{16G_m^*(\omega)+19G_d^*(\omega)\}}{40\left(\frac{\Gamma}{R_v}\right)\{G_m^*(\omega)+G_d^*(\omega)\}+\{2G_d^*(\omega)+3G_m^*(\omega)\}\{16G_m^*(\omega)+19G_d^*(\omega)\}} \tag{7}$$

$$R_V = \frac{\sum(R_i \times \phi_i)}{\phi} \tag{8}$$

where $G_d^*(\omega), G_m^*(\omega)$, and $G^*(\omega)$ are the complex shear moduli of dispersed phase, continuous phase, and the blend, respectively, at frequency ω; Γ is the interfacial tension; and ϕ and R_V are the volume fraction and the volume average radius, respectively, of the dispersed phase. The R_V for each blend system is determined by SEM observation as mentioned later.

Figure 3 compares the oscillatory shear moduli evaluated by the emulsion model, illustrated by the solid lines, with the experimental values for the blends at 180 ºC. As shown in the figure, the predicted values, assuming that the interfacial tension between PLA and PBS is 3.5 [mN/m], are in a good agreement with the experimental data irrespective of the blend ratio. Since interfacial tension is basically independent of viscosity ratio of the components and blend ratio, the value would be available for the prediction of morphology for various PLA/PBS blend systems.

[Figure 3]

Dynamic Mechanical Properties in Solid Sate

Dynamic mechanical properties in the solid state are investigated employing the flat sheets obtained by the compression-molding. The temperature dependence of the dynamic tensile moduli for PLA, PBS, and the blends is shown in Figure 4.

[Figure 4]

The storage modulus E' of PLA falls off sharply around at 60 ºC due to the glass transition and then increases again between 100 and 120 ºC, which corresponds with the previous reports [18,21]. The increase in E' around at 100 ºC for PLA is ascribed to the crystallization. Since the material cannot crystallize enough at the sample preparation condition (cooled at 40 ºC) due to the slow crystallization rate, the crystallization takes place beyond the glass transition temperature at the heating process of the measurement. This phenomenon is called as “cold crystallization” [22]. The

occurrence of the cold crystallization indicates that the cooling condition of the processing method employed in this study is “quench” for PLA. Finally, E' drops rapidly with temperature around at 150 ºC owing to the melting of crystal. As for PBS, the peak due to the glass transition in the E'' curve is located around at -30 ºC with less intense fashion than that for PLA. This is reasonable because the degree of crystallization for PBS is considerably higher than that for PLA. Further, E' decreases moderately with temperature and falls off sharply at 100 ºC. In case of the blends, it is found that there appear double peaks in the E'' curve in the temperature region between -30 and 60 ºC. The lower peak becomes weak with decreasing PBS content in the blends. Further, the peak temperature due to the glass transition of PLA is independent of the blend ratio, suggesting that mutual dissolution does not take place.

Besides the dynamic mechanical measurements, phase separation is confirmed by SEM pictures as depicted in Figure 5. It is found that spherical PBS droplets with smooth surface are found in a continuous phase. The volume average radii of the dispersed particles *Rv* are 0.98 μm for PLA/PBS (80/20), 0.52 μm for PLA/PBS (90/10), and 0.27 μm for PLA/PBS (95/5). The radii are applied for the calculation of the emulsion model.

[Figure 5]

Figure 4 also demonstrates that the enhancement of E' due to the cold-crystallization of PLA is shifted to lower temperature by blending PBS. This phenomenon indicates that PBS accelerates the cold-crystallization of PLA as pointed in the previous works [18,21].

For the better understanding of the cold-crystallization, thermal analysis is performed. Figure 6 shows DSC heating curves of PLA, PBS, and the blends at a heating rate of 2 ºC/min, *i.e.*, the same rate as the dynamic mechanical analysis. The DSC curves demonstrate that the glass transition temperature (Tg) of PLA, denoted by the small arrow in the figure, is around 60 ºC, corresponding with the dynamic mechanical spectra. Further, PLA has a crystallization peak at 110 ºC and shows double peaks around at 150 ºC due to melting in the DSC heating curve. The melting peak located at the lower temperature is attributed to less organized crystals that would be formed during the DSC measurement. It should be noted that the melting peak at the higher temperature of the blends is pronounced, suggesting that the blends have well-organized crystals compared with the pure PLA. Furthermore, the exothermic peak ascribed to the cold-crystallization, indicated by the bold arrows, is located at lower temperature than that of the pure PLA, as detected by the dynamic mechanical measurements. The endothermic peak around at 110 ºC is attributed to the melting peak of PBS. The location of PBS melting peak for the blends is the same as that for the pure PBS.

[Figure 6]

Crystallization Behavior

The enhancement of cold crystallization of PLA suggests that PBS droplets act as crystallization nucleus for PLA. The small amount of crystallites formed at the cooling process, in which PBS particles would act as nuclei, accelerates the crystallization during heating process. In order to confirm the nucleating ability of PBS,

crystallization behavior of the blend is studied by means of DSC and an optical polarized microscope with a hot stage.

Figure 7 shows DSC cooling curves for PLA and the blends at a cooling rate of 2 ºC/min. Although it is not presented in the figure, there is a sharp and pronounced peak due to crystallization for PBS at 85 ºC. On the contrary, PLA shows no crystallization peak, because the cooling rate in this experiment is too fast for PLA to crystallize. This is one of the most serious problems for the industrial application of PLA, leading to intensive R&D activities in industries to improve commercially available nucleating agents having insufficient ability. As for the cooling curves of the blends, however, the crystallization peak is clearly detected around at 90 ºC, demonstrating that PBS droplets act as nucleating entities for PLA. Regardless of the weak nucleating effect as compared with the conventional nucleating agents [7-9], this is quite interesting phenomena because PBS is in a molten state at the temperature.

[Figure 7]

The crystallization process is observed also by an optical microscope at the same cooling rate. Figure 8 shows the optical micrographs under crossed polars at 100 ºC. As shown in the figure, numerous bright spots due to PLA crystallites are clearly detected in the blends, whereas the crystallization does not occur for the pure components such as PLA and PBS. In case of PBS, bright spots appear suddenly at 85 ºC. Similar behavior was reported by Jiang et al. [38] for the blend of PLA and poly(butylene adipate-co-terephthalate) PBAT, although there was no optical micrograph for pure PBAT.

[Figure 8]

Both DSC and optical microscope measurements directly reveal that crystallization of PLA is accelerated by the existence of PBS even in a molten state. The result suggests that molten PBS and/or impurities in the original PBS act as crystallization nuclei for PLA. The nucleating effect of PBS, leading to the generation of crystalline embryos of PLA at the quench condition, will be responsible for the pronounced cold-crystallization and the increment of the modulus beyond the glass transition temperature as detected at the dynamic mechanical measurements.

CONCLUSION

Structure and properties for binary blends of PLA and PBS are studied both in the solid and molten states. It is found that PLA and PBS are immiscible in the molten state and the blends exhibit phase-separated structure. The interfacial tension between PLA and PBS is estimated using a rheological emulsion model proposed by Palierne and found to be 3.5 [mN/m]. In this study, basic rheological parameters are also evaluated for PLA and PBS. It is suggested that the entanglement molecular weight of PLA is lower than that of PBS.

Further, there are distinct double peaks in the dynamic mechanical spectra ascribed to the glass transition of each component. Since the peak temperature of the E'' curve is located at those of the individual pure components, mutual dissolution dose not take place in the blends. Blending PBS, however, accelerates the crystallization

of PLA, which is directly detected by DSC and optical microscope measurements at the cooling process. This is a significantly interesting phenomenon because molten PBS droplets act as crystallization nucleus for PLA. Furthermore, the PLA crystallites generated during the quench operation are responsible for the enhancement of the cold crystallization behavior for the blends.

REFERENCES

[1] Fomin VA, Guzeev VV. Rub Chem Technol 2001;17:186.

[2] Doi Y, Steinbuchel A. Biopolymers Vol. 3b and 3c, New York: Wiley-VCH; 2002.

[3] Arakawa K, Yokohara T, Yamaguchi M. J Appl Polym Sci 2007;107:1320.

[4] Ogata N, Jimenez G, Kawai H, Ogihara T. J Polym Sci Polym Phys 1997;35:389.

[5] Ray SS, Bousmina M. Prog Materials Sci 2005;50:962.

[6] Nam JY, Okamoto M, Okamoto H, Nakano M, Usuki A, Matsuda M. Polymer 2006;47:1340.

[7] Kawamoto N, Sakai A, Horikoshi T, Urushihara T, Tobita E. J Appl Polym Sci 2007;103:244.

[8] Liao R, Yang B, Yu W, Zhou C. J Appl Polym Sci 2007;104:310.

[9] Niga S, Yoshimura M, Yanase H. Prep Ann Meeting Soc Polym Sci Jpn 2006;Sep:1228.

[10] Yamane H, Sakai K. Polymer 2003;44:2569.

[11] Ikeda Y, Jamshidi K, Tsuji H, Hyon S H. Macromol 1987;20:904.

[12] Anderson KS, Hillmyer MA. Polymer 2006;47:2030.

[13] Bluemm E, Owen AJ. Polymer 1995;36:4077.

[14] Koyama N, Doi Y. Polymer 1997;38:1589.

[15] Ohkoshi I, Abe H, Doi Y. Polymer 2000;41:5985.

[16] Ferreira BMP, Zavaglia CAC, Duek EAR. J Appl Polym Sci 2002;86:2898.

[17] Park JW, Im SS. J Appl Polym Sci 2002;86:647.

[18] Takagi J, Nemoto T, Takahashi T, Taniguchi T, Koyama K. Seikei-Kakou 2003;15:581.

[19] Hirotsu T, Nakayama K, Tagaki C, Watanabe T. J Photopolym Sci Technol

2004;17:179.

[20] Chen GX, Kim HS, Kim ES, Yoon JS. Polymer 2005;46:11829.

[21] Shibata M, Inoue Y, Miyoshi M. Polymer 2006;47:3557.

[22] Wunderlich B. Thermal Analysis of Polymeric Materials. Berlin: Springer-Verlag; 2005.

[23] Taylor GI, Proc R Soc London 1932;A138:41.

[24] Tokita N, Pliskin I. Rub Chem Technol 1973;46:1166.

[25] Grace HP. Chem Eng Commun 1982;14:225.

[26] Wu S. Polym Eng Sci 1987;27:335.

[27] Meijer HE, Janssen JMH. Mixing of Immiscible Liquids; in Mixing and Compounding of Polymers, Chap.4, Eds. Manas-Zloczower I, Tadmor Z. Munich: Hanser; 1994.

[28] Ferry JD. Viscoelastic Properties of Polymers. 3rd Edition. New York: Wiley; 1980.

[29] Mills NJ. Nature 1968;219:1219.

[30] Graessley WW. J Chem Phys 1971;54:5143.

[31] Graessley WW. Adv Polym Sci 1974;16:1.

[32] Oldroyd JG.. Proc R Soc A 1953;218:122.

[33] Pelierne JF. Rheol Acta 1990;29:204.

[34] Graebling D, Muller R, Palierne JF. Macromolecules 1993;26:320.

[35] Doi M, Ohta T. J Chem Phys 1991;95:1242.

[36] Yamaguchi M. J Appl Polym Sci 1998;70:457.

[37] Yamaguchi M, Miyata H. Macromolecules 1999;32:5911.

[38] Jiang L, Wolcott MP, Zhang J. Biomacromolecules 2006;7:199.

Figure Captions

Figure 1 Master curves of frequency dependence of shear storage modulus G' (open symbol) and loss modulus G'' (closed symbol) for (a) PLA and (b) PBS; (triangles) 160 ºC, (circles) 180 ºC, (squares) 200 ºC, and (diamonds) 220 ºC. The reference temperature is 180 ºC.

Figure 2 Master curves of frequency dependence of shear storage modulus G' (open symbol) and loss modulus G'' (closed symbol) for (a) PLA/PBS (80/20), (b) PLA/PBS (90/10), and (c) PLA/PBS (95/5); (triangles) 160 ºC, (circles) 180 ºC, (squares) 200 ºC, and (diamonds) 220 ºC. The reference temperature is 180 ºC.

Figure 3 Comparison of the experimental data (circles) with the predicted values by the rheological emulsion model (solid lines) at 180 ºC for (a) PLA/PBS (80/20), (b) PLA/PBS (90/10), and (c) PLA/PBS (95/5).

Figure 4 Temperature dependence of (a) tensile storage modulus E' and (b) loss modulus E'' at 10 Hz for PLA ($\alpha = 0$), PLA/PBS (95/5) ($\alpha = 2$), PLA/PBS (90/10) ($\alpha = 4$), PLA/PBS (80/20) ($\alpha = 6$), and PBS ($\alpha = 8$).

Figure 5 Scanning electron micrographs of (a) PLA/PBS (80/20), (b) PLA/PBS (90/10), and (c) PLA/PBS (95/5).

Figure 6 DSC heating curves of PLA, PBS, and the blends at a heating rate of 2 ºC/min. The small arrow in the figure represents the glass transition of PLA and the bold arrows denote the cold-crystallization.

Figure 7 DSC cooling curves for PLA and PLA/PBS blends at a cooling rate of 2 ºC/min. The arrows in the figure indicate the crystallization peaks for PLA.

Figure 8 Polarized optical micrographs under crossed polars at 100 ºC at the cooling process for PLA, PBS, and the blends.

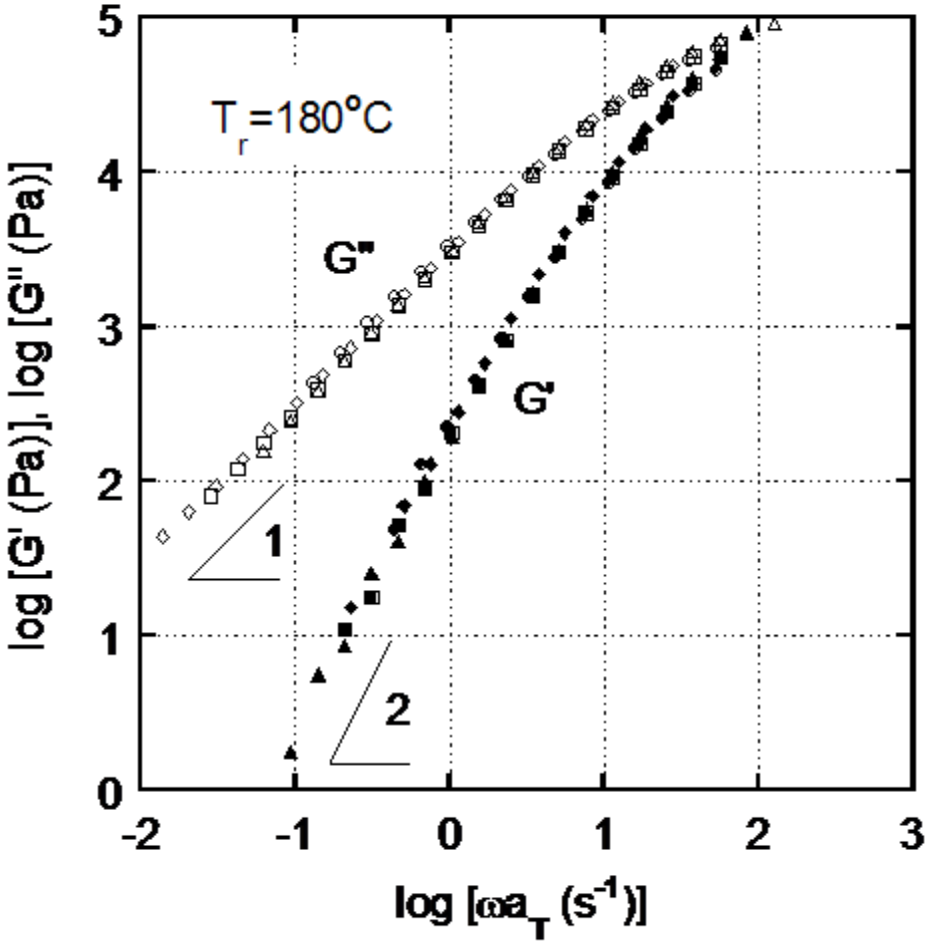

Figure 1(a)

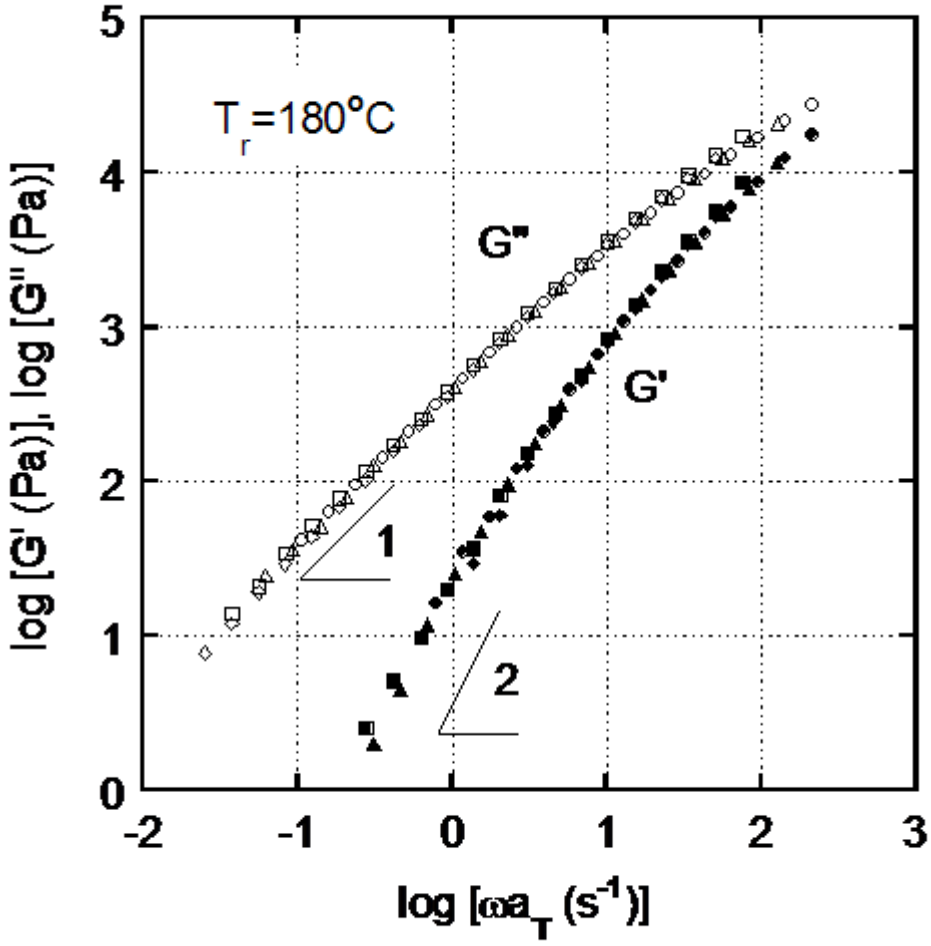

Figure 1(b)

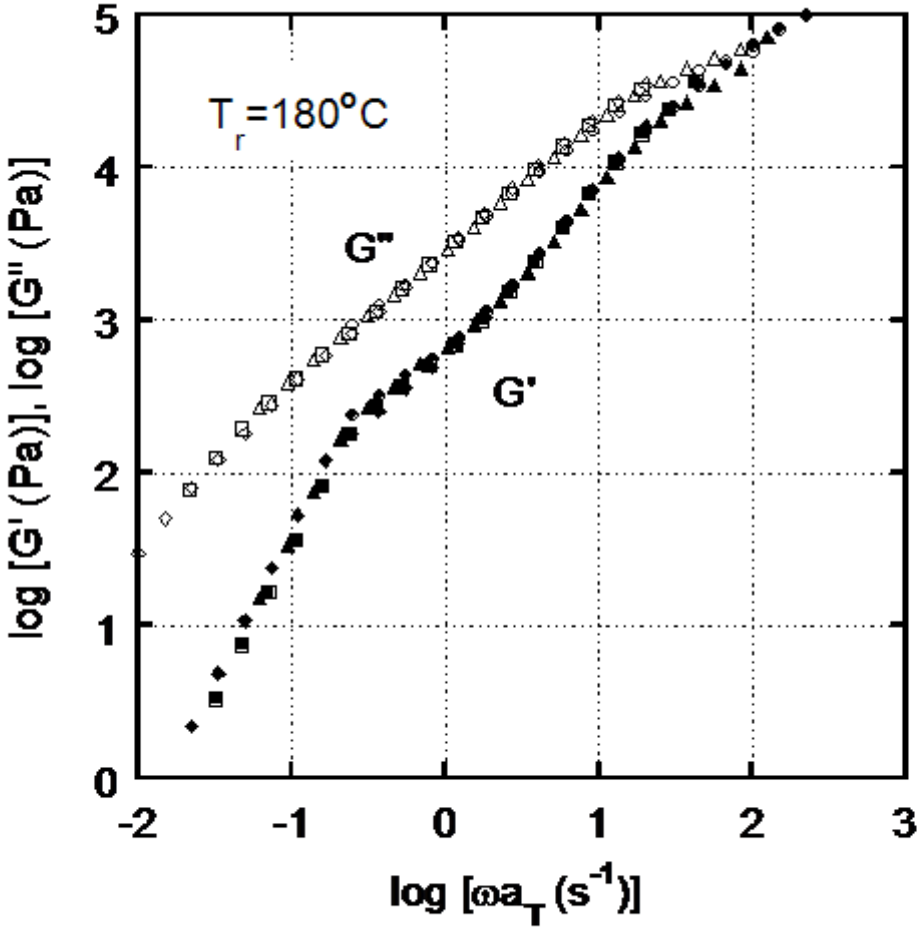

Figure 2(a)

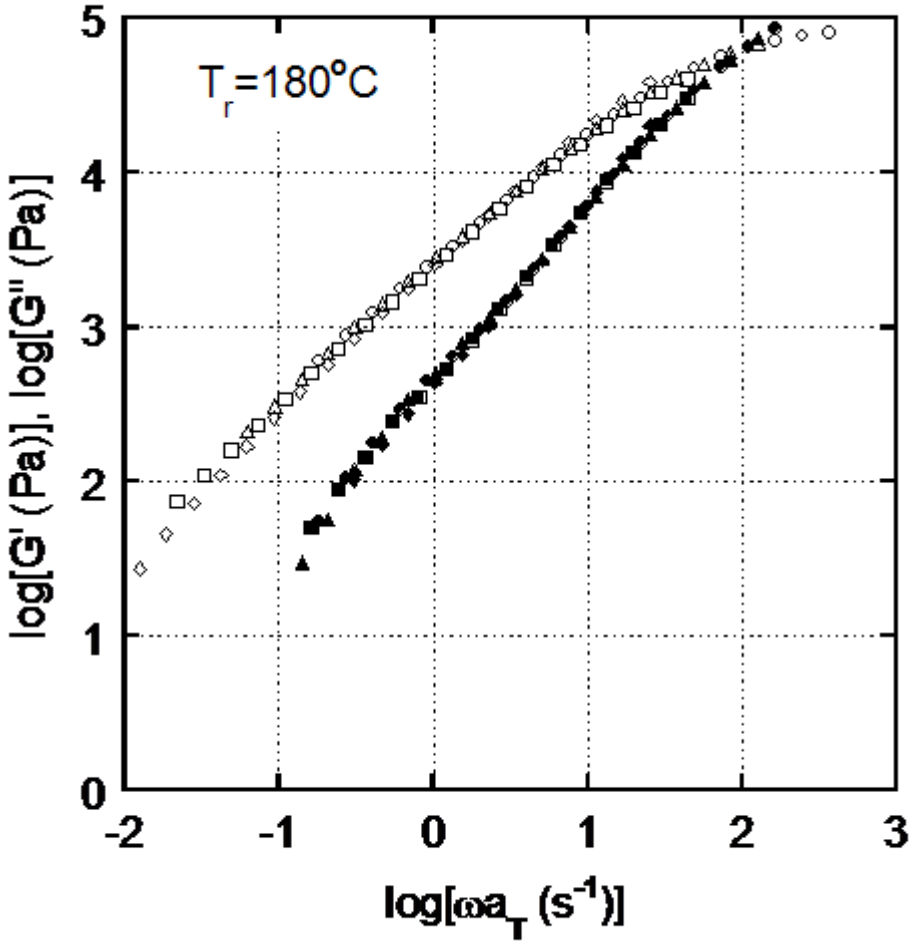

Figure 2(b)

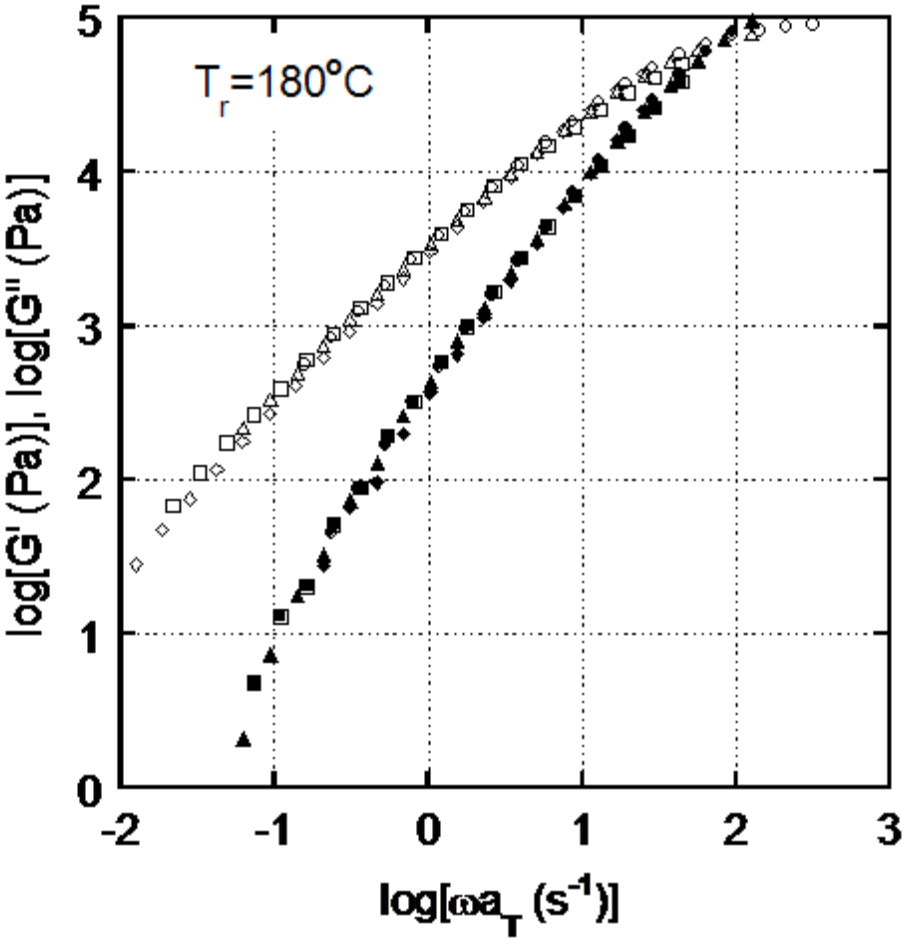

Figure 2(c)

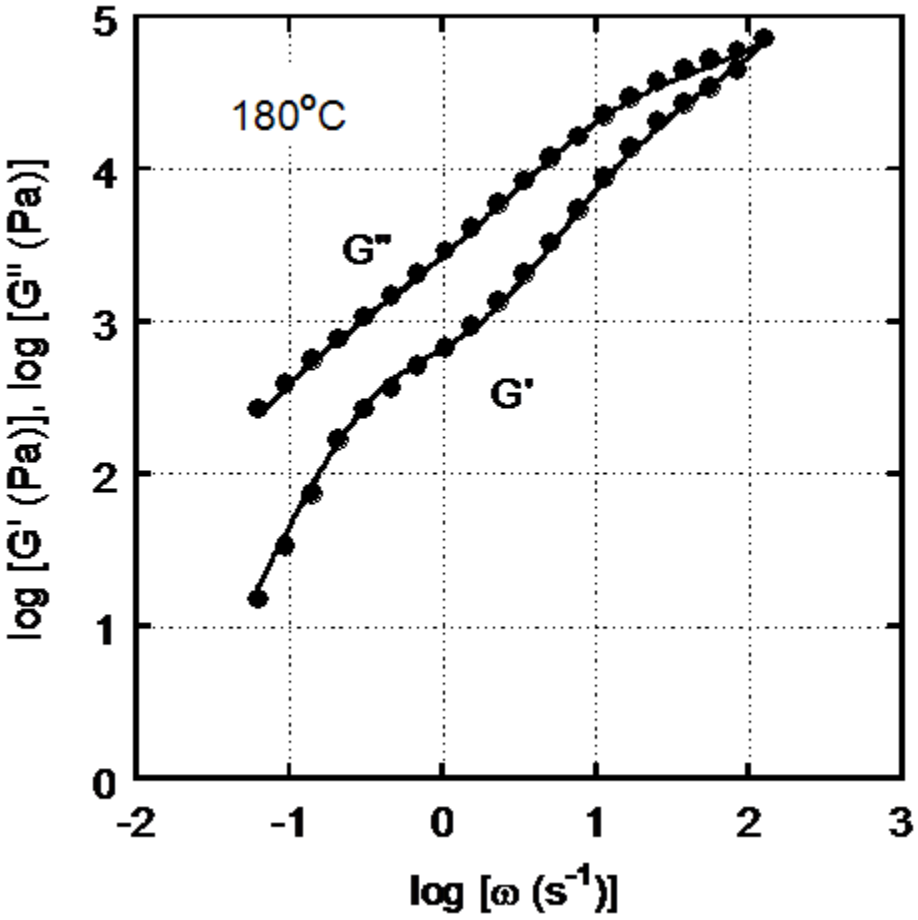

Figure 3(a)

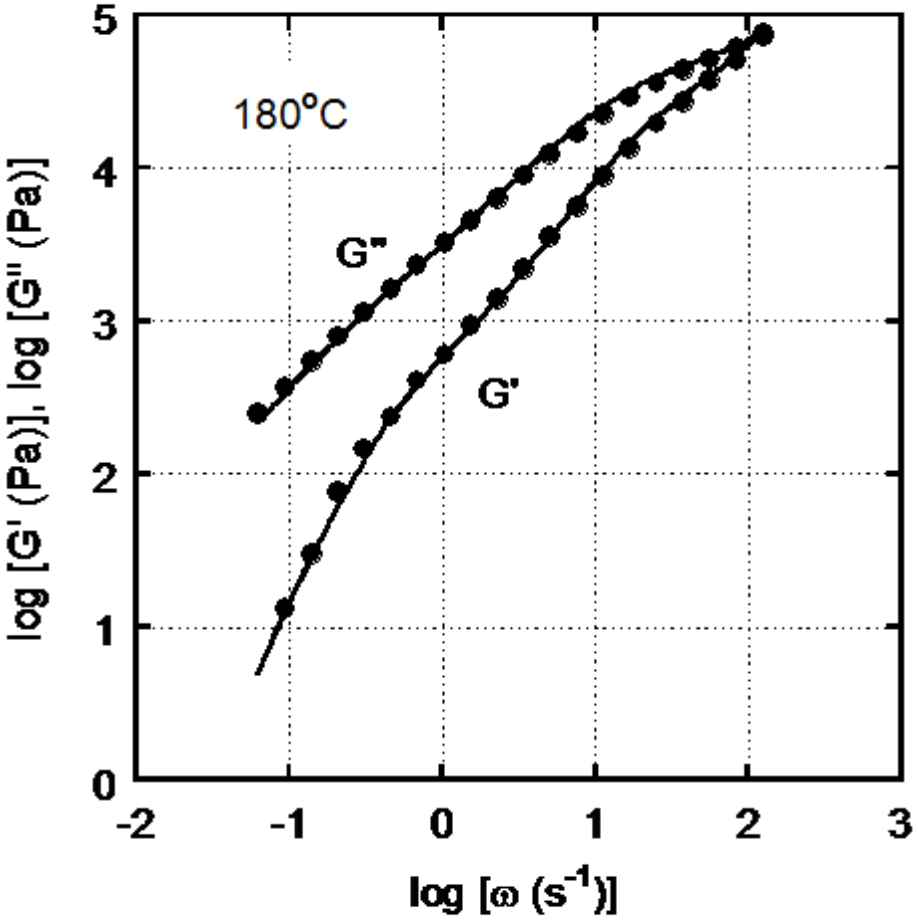

Figure 3(b)

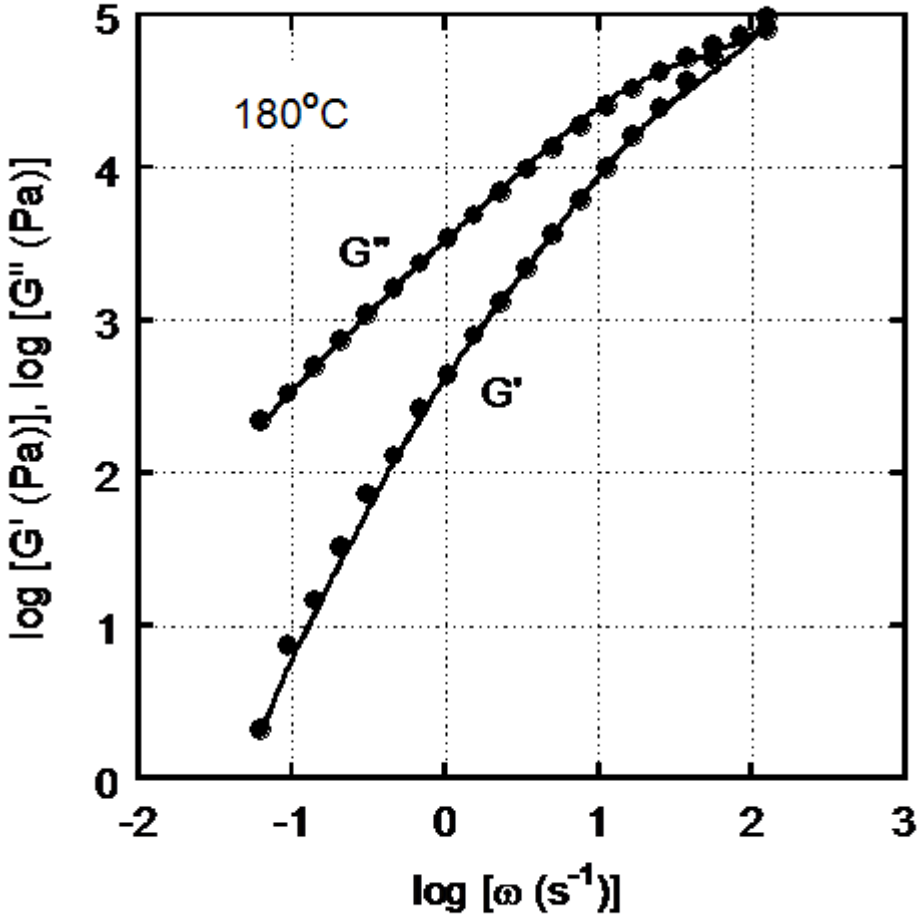

Figure 3(c)

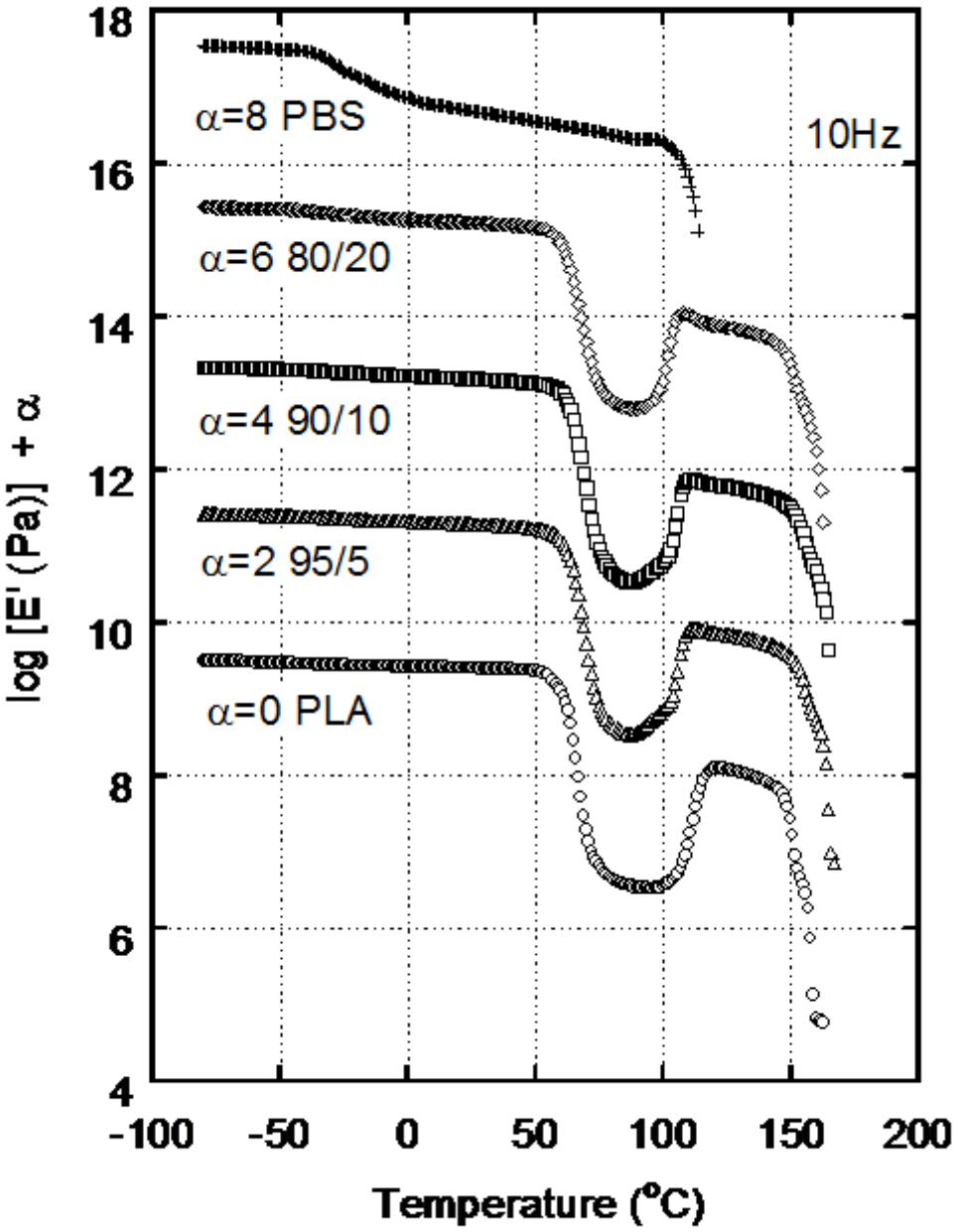
18
16
14
12
10
8
6
4
log [E' (Pa)] + α
α=8 PBS
10Hz
α=6 80/20
α=4 90/10
α=2 95/5
α=0 PLA
-100
-50
0
50
100
150
200
Temperature (°C)

Figure 4(a)

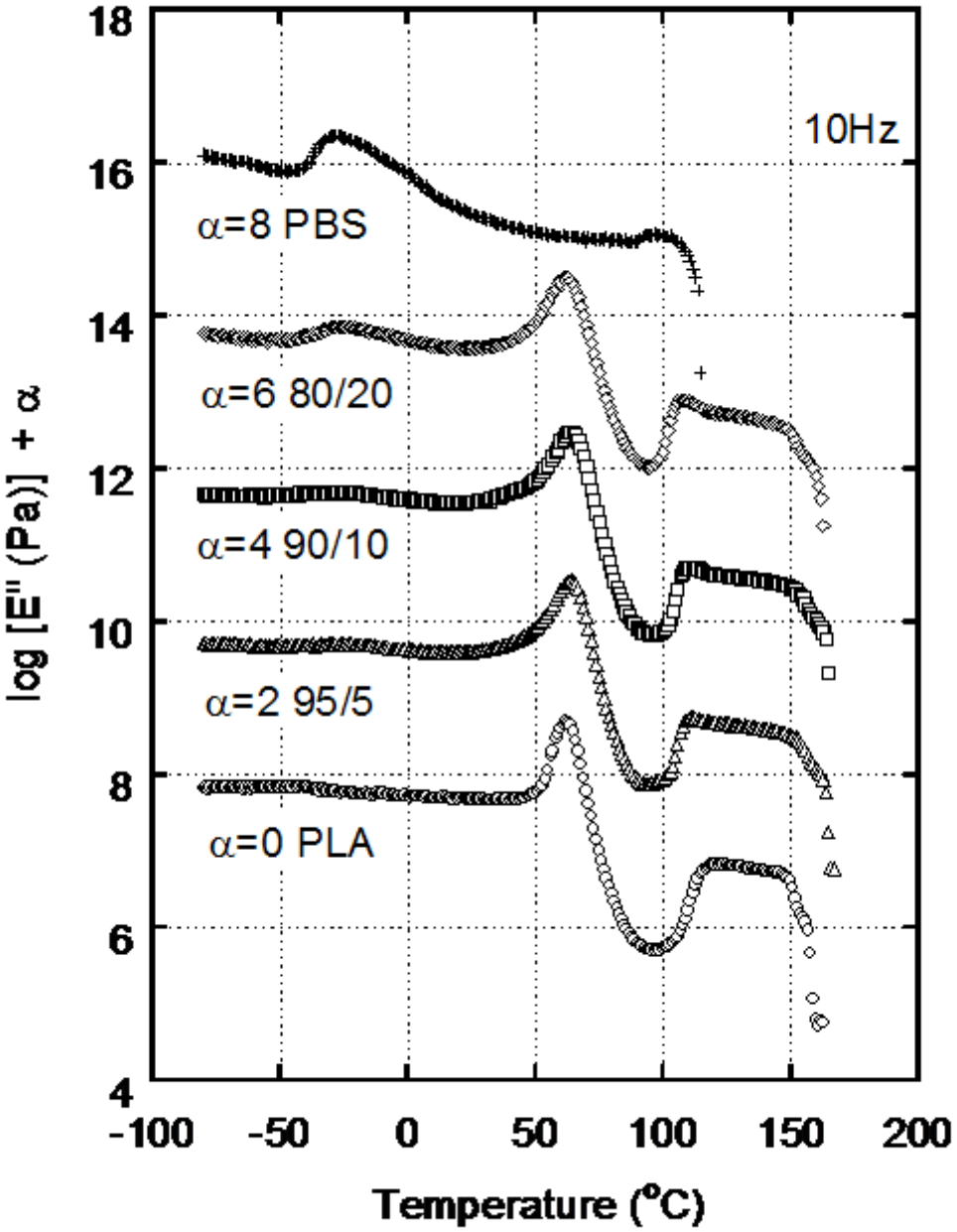
10Hz
α=8 PBS
α=6 80/20
α=4 90/10
α=2 95/5
α=0 PLA
log [E'' (Pa)] + α
Temperature (°C)
18
16
14
12
10
8
6
4
-100
-50
0
50
100
150
200

Figure 4(b)

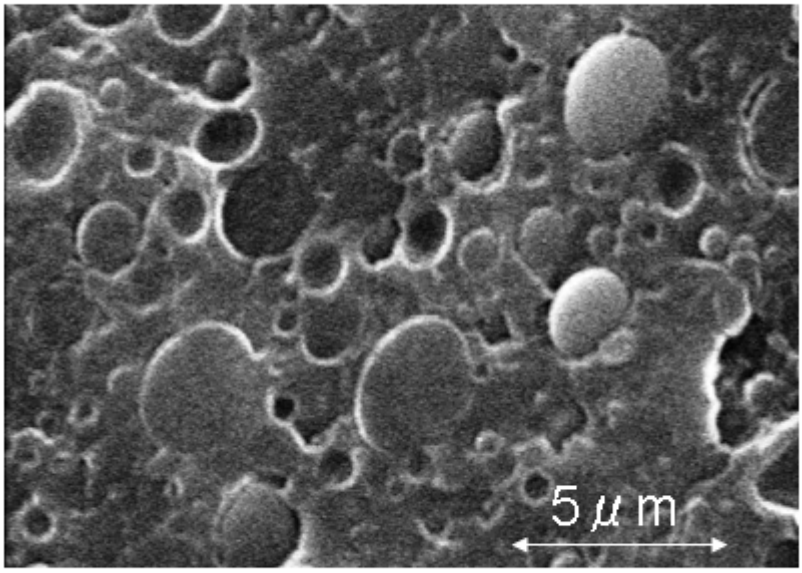

Figure 5(a)

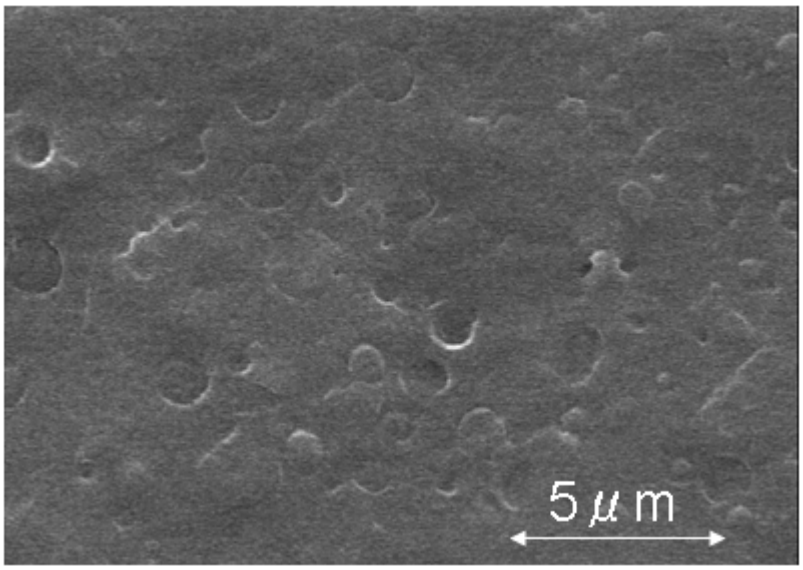

Figure 5(b)

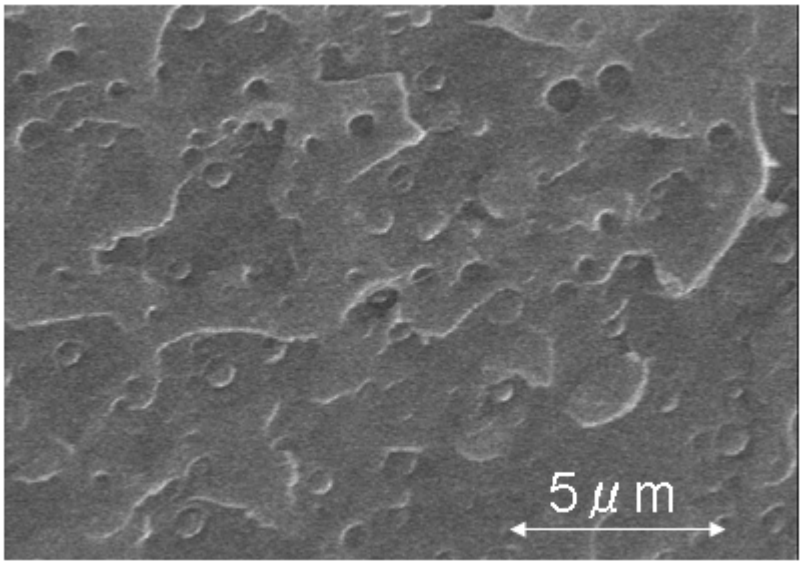

Figure 5(c)

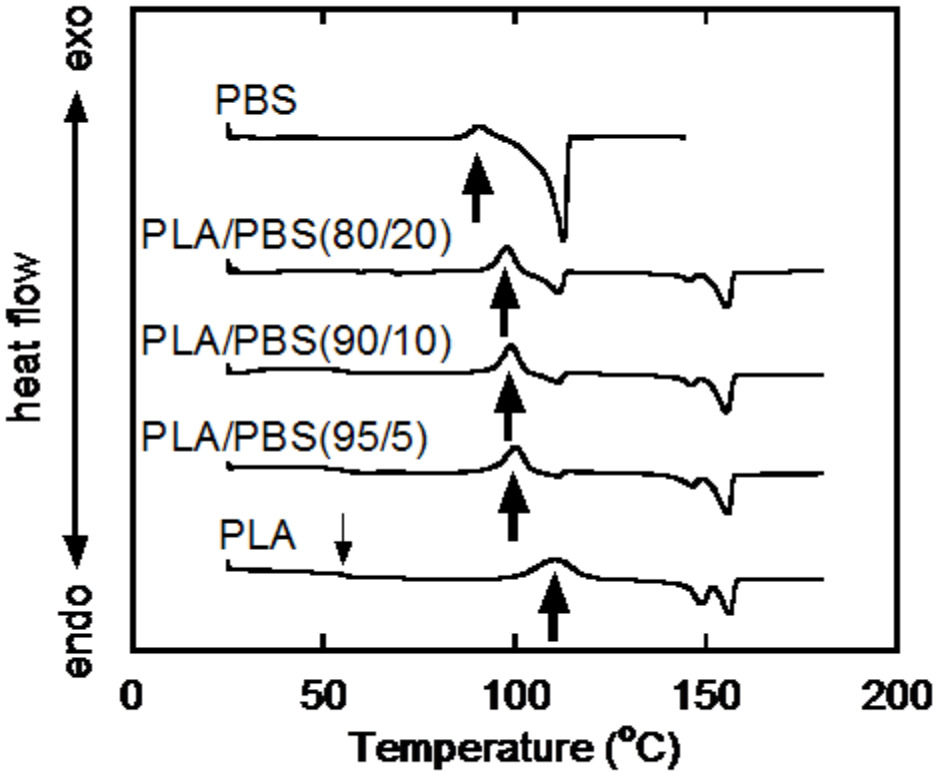
exo
heat flow
endo
PBS
PLA/PBS(80/20)
PLA/PBS(90/10)
PLA/PBS(95/5)
PLA
0
50
100
150
200
Temperature (°C)

Figure 6

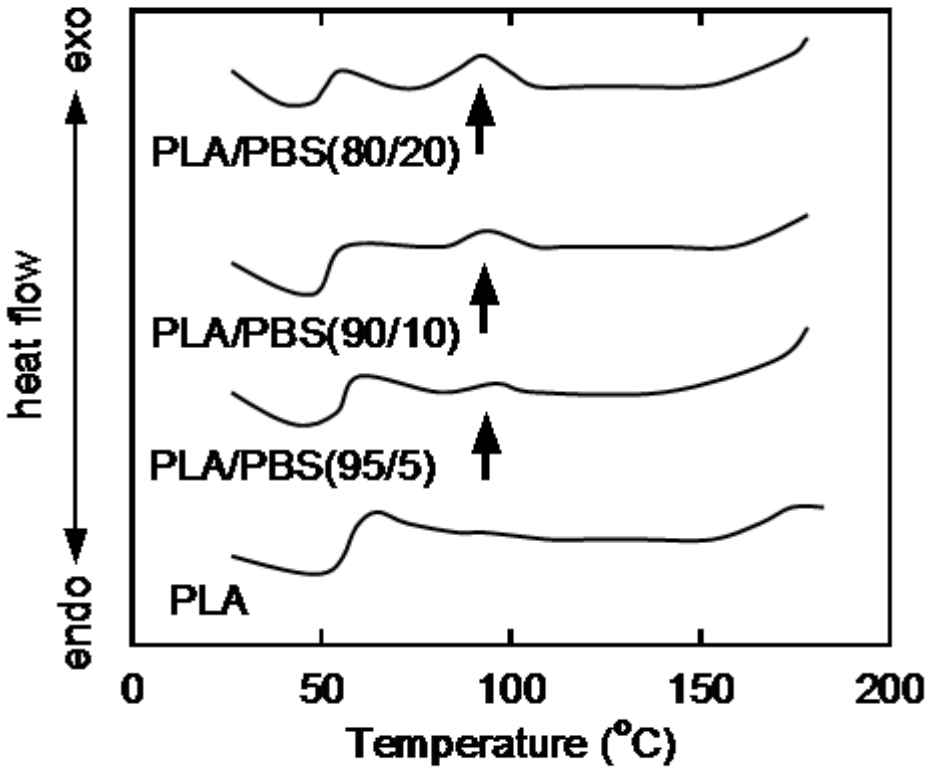
exo
heat flow
endo
PLA/PBS(80/20)
PLA/PBS(90/10)
PLA/PBS(95/5)
PLA
0
50
100
150
200
Temperature (°C)

Figure 7

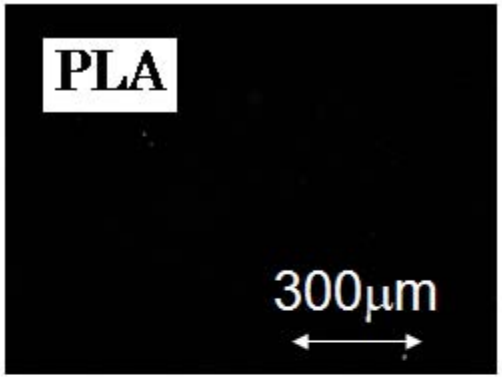
PLA
300μm

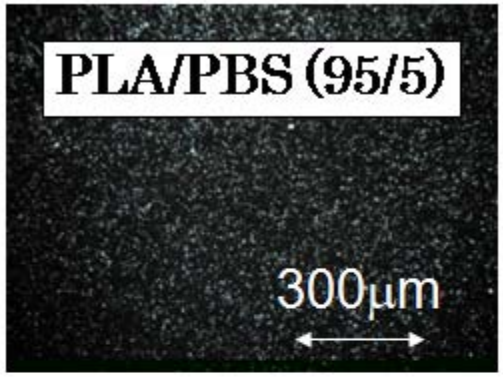
PLA/PBS (95/5)
300μm

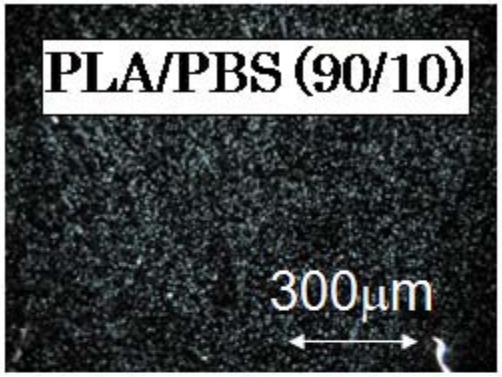
PLA/PBS (90/10)
300μm

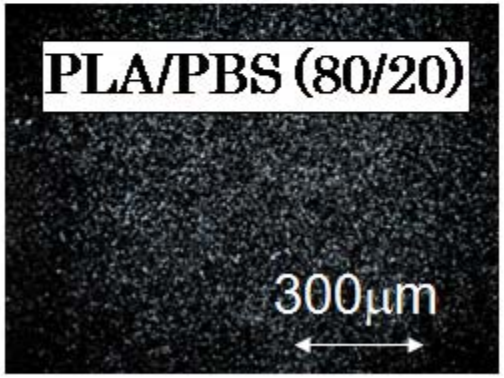
PLA/PBS (80/20)
300μm

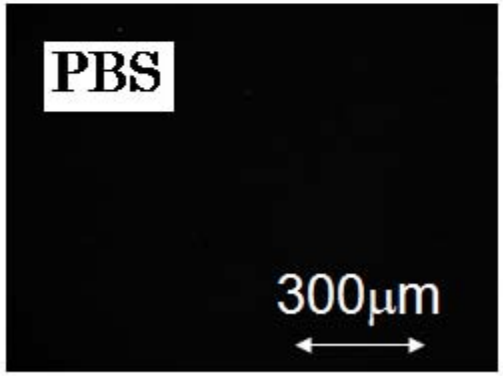
PBS
300μm

Figure 8